Full-potential linear-muffin-tin-orbital study of brittle fracture in titanium carbide

David L. Price
Department of Physics, Memphis State University, Memphis, Tennessee 38152

Bernard R. Cooper
Department of Physics, West Virginia University, Morgantown, West Virginia 26506

John M. Wills
Los Alamos National Laboratory, Los Alamos, New Mexico 87545
(Received 24 July 1992)

The inelastic behavior of the refractory transition-metal carbides is dominated, at low temperatures, by brittle fracture. We discuss in this article our theoretical study of both the elastic and fracture properties of titanium carbide under tensile stress. The calculations involved were performed using a full-potential linear-muffin-tin-orbital electronic structure method, with a repeated slab arrangement of atoms simulating an isolated cleavage plane. We report results for the elastic constants (excluding the shear modulus), the stress-strain relationship up to the point of fracture, and the ideal yield stress and strain for stoichiometric TiC. We relate these properties to the details of the electronic structure and to the breaking of metal-nonmetal covalent bonds at the cleavage plane. This includes a detailed pictorial analysis of the charge redistribution accompanying cleavage.

I. INTRODUCTION

The transition-metal carbides are a class of very hard materials, with exceptionally high melting temperatures.[1] They are also very brittle materials and provide one of the better examples of a fracture which is almost entirely brittle in nature. While they exhibit a number of unusual properties, most applications of the transition-metal carbides rely upon their extreme hardness; for example, they are widely used as the main constituent in metal cutting tools. The primary limiting factor in these high-stress applications is the brittleness of the materials, and so the fracture properties of the carbides are of some practical interest. In this paper we examine the brittle cleavage fracture of stoichiometric TiC under tensile stress.

Titanium carbide and the other cubic carbides have (001) cleavage planes[2] and fracture along these planes in a brittle manner up to relatively high temperatures, with a brittle to ductile transition occurring at about 800 °C.[1] The experimental tensile yield stresses of TiC samples can vary greatly since, in practice, cleavage under tensile stress is nucleated by preexisting cracks or other defects. As a result, the limiting yield stress of the ideal crystal (which is typically estimated[3] to be some fraction of the Young's modulus, E, such as $E/20$ or $E/10$) is never obtained in real samples. The range of actual yield stresses in TiC range from $\frac{1}{100}$ to $\frac{1}{4}$ of the estimated ideal yield stress. While significant progress is currently being made in atomic scale calculations of fracture processes,[4] inclusion of realistic material characteristics in first-principles calculations remains very difficult, and in this article we discuss calculations which are restricted to the fracture properties of ideal crystalline TiC. While such calculations cannot be compared directly to the fracture properties of real TiC samples, they nonetheless are of interest for a number of reasons. One is that the calculation provides a value for the intrinsic strength and so provides an upper limit for the true yield stress. The ideal yield stress is also a quantity which appears in many theories of propagation of cracks. In addition, such calculations as the one described below allow investigation into the relationship of the fracture properties of TiC to its electronic structure, and provide a point of comparison for the later calculations which will examine the effect of carbon vacancies on the ideal yield stress. Indeed, we believe that the greatest benefit of the present work is its value in helping to uncover, and allow the visualization of, the atomic origins of bond failure in fracture. We believe that the detailed figures showing election density behavior of specific states as fracture proceeds, discussed in Sec. II B, should be especially helpful in that regard.

Our method of calculation is a full-potential variation of the standard linear-muffin-tin-orbital (LMTO) electronic structure method,[5] and has been described in greater detail elsewhere.[6,7] The method, as used here, is capable of dealing with very open systems, such as surfaces, while at the same time it is not constrained to surface situations, so that a continuous transition from a bulk, closely packed arrangement of atoms to an open arrangement, such as when a cleavage plane is created, is easily dealt with. The creation of a cleavage plane is achieved in this calculation by using a repeated slab arrangement of atoms, with four layers of TiC per slab. Other technical details of the calculation are discused below where they are relevant.

Our discussion of the calculated results proceeds as follows. We first (Sec. II A) discuss the stress-strain relationship and elastic constants of bulk TiC. The calculated bulk modulus, Young's modulus, and Poisson's ratio

(only two of which are independent) are compared to experimental values, and, in addition to this, we pursue the stress-strain relationship out to relatively absurd values of strain in order to facilitate evaluation of the inelastic behavior of TiC. Next, in Sec. II B, we investigate in detail an idealized cleavage process in TiC, in which a (001) cleavage plane is opened up, while the remaining lattice is maintained at its equilibrium configuration. This is done using the four-layer repeated slab construction, and it provides a first estimate of the ideal yield stress and strain, the cleavage energy, and a microscopic view of the cleavage process. This part of the calculation also provides, at large values of cleavage separation, a calculation of titanium carbide (001) surface properties. Following this, we describe a calculation combining the two calculational techniques and results discussed in Secs. II A and II B to obtain what is, in principle, a proper determination of the ideal stress of TiC. Section III contains a summary.

II. RESULTS

A. Bulk elastic constants, stress-strain relationship

The results reported in this section are restricted to the elastic behavior of bulk TiC, including its response to extreme tensile stress. Tensile stress along the [001] direction deforms the interpenetrating fcc lattices of TiC's NaCl structure into body-centered tetragonal form, and the total energy of the two-atom unit cell with that structure was calculated for a range of the c and a lattice parameters. The calculation was performed with a basis set as flexible as that used in the surface-type calculations described in Sec. II B, so that, as the crystal was stretched, creating very open interstitial regions, no expansion of the basis set was required.

For evaluation of the elastic constants, the total energy was calculated over a square grid in the plane of the c and a lattice constants. The fractional change allowed in the lattice constants was relatively small (from 7.8 to 8.4 a.u. for both a and c or about 4% of the equilibrium lattice constant), and the elastic constants were obtained by fitting the calculated energies to a cubic polynomial in the two variables. We have made no great effort to maximize the accuracy of the calculated elastic constants (for example, only 18 special points in the irreducible wedge of the Brillouin zone were used). As a result, based upon the experience of ourselves and others in calculating these quantities, we expect fairly accurate results (within about 2%) for quantities involving the first derivative of the energy, such as equilibrium lattice constants, while quantities involving second derivatives of the calculated energy (such as the bulk modulus and Young's modulus) can be expected to have uncertainties of about 20%. The calculated lattice constants and elastic parameters, which are listed and compared to experiment in Table I, are in accord with these expectations.

For larger values of strain along the [001] direction, we have, at selected values of the c lattice parameter, calculated the total energy as a function of the second lattice parameter, a, and so obtained the equilibrium value of a and the energy as functions of tensile strain. Figures 1 and 2 summarize the results of this procedure. Figure 1 shows the equilibrium value of the a lattice constant as a function of c, from values of c slightly smaller than the experimental value out to a value of 18 a.u., corresponding to a strain of over 100%. The dashed line in this figure shows the linear a versus c relationship corresponding to the calculated value of the Poisson ratio listed in Table I (which is within 10% of the experimental result), and the solid line is a simple function (polynomial times exponential) fitted to the calculated points. Deviations from linearity are small for strains less than about 5%; but the value of a is clearly nearing its asymptotic limit, that associated with a single isolated (001) plane of TiC, within the limits of the graph. By extrapolation, the asymptotic value of a is 7.80 a.u. Figure 2 shows the total energy as a function of the c lattice constant. The minimum and second derivative at the minimum give a second determination of the lattice constant and Young's modulus, and differ from the values listed in Table I by less than 1%. The total energy difference required to pull

TABLE I. Comparison of calculated and experimental quantities.

	Calc.	Expt.
Lattice const. (a.u.)	8.07	8.18[a]
c/a ratio	1.000	1.000
Bulk mod. (dyn/cm^2)	3.1×10^{12}	(2.4×10^{12})[b]
Young's mod. (dyn/cm^2)	5.6×10^{12}	(4.8×10^{12})[b]
Poisson ratio	0.19	0.17[b]
Frac. stress (dyn/cm^2)	4.3×10^{11}	(0.55×10^{11})[c]
Frac. strain	18%	1.2%[c]
Surface energy (erg/cm^2)	3270	

[a]Reference 8.
[b]Reference 9.
[c]Reference 4.

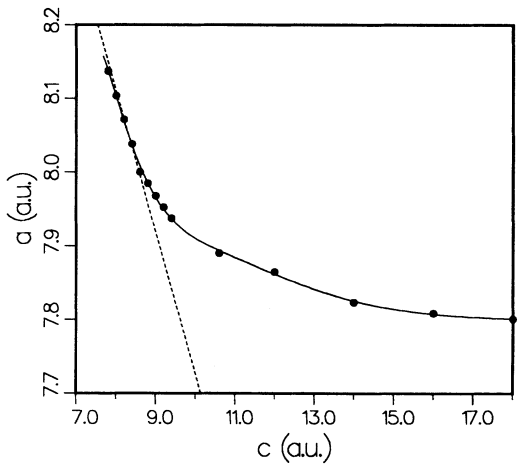

FIG. 1. The calculated equilibrium a lattice constant in the stretched NaCl structure of TiC, as a function of the c lattice constant. The dashed line corresponds to the value of the Poisson ratio calculated by examining energies near the equilibrium lattice structure.

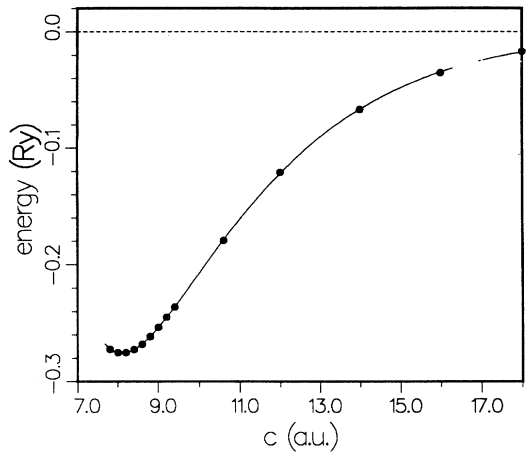

FIG. 2. The calculated total energy of the stretched TiC crystal as a function of the c lattice constant. The solid line is a least-squares fit and the dashed line is the asymptotic value of the fitted curve.

TiC into separate (001) planes is evaluated to be 8.4×10^{-3}Ry/a.u.^{2} (6560 erg/cm^2) and the inflection point in the curve, which occurs at a strain of 22% ($c=9.9$ a.u.), gives a maximum stress at this point of 4.4×10^{11} dyn/cm^2. (The complete stress-strain relationship is given below.) It is at this value of strain that the crystal is unstable with respect to unlimited stretching under conditions of constant applied stress. For an infinite length of material, the system is, for any finite strain, only metastable, the absolute equilibrium state being one in which the sample has cleaved into two sections, both at the equilibrium (zero-pressure) lattice constants. The question we begin to address in Sec. II B is where along such a curve as shown in Fig. 2 does an ideal crystal (at zero temperature) lose its metastability against cleavage and so fracture?

B. (001) fracture of TiC

The repeated slab construction used to study the cleavage of TiC is depicted in Fig. 3. Each unit cell contains one "slab" and each slab consists of four layers of (001) planes of TiC. Choosing an even number of slabs simplifies the symmetries, given the $ABAB$ stacking of (001) planes in the rocksalt structure. The simulation of the separation of two neighboring planes is accomplished by varying the separation, S, between the slabs. Thus, for $S=0$ we simply have bulk TiC, and as S is increased we slowly separate the slabs, until, at large separations we have a repeated slab calculation of isolated surfaces. Before looking at the separation process itself, we shall briefly describe the surface properties obtained at the largest value of the separation considered ($S=7.36$ a.u.).

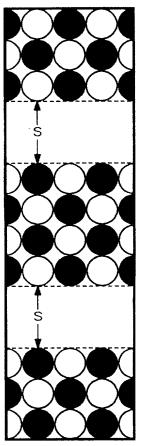

FIG. 3. A depiction of the atomic arrangement used for simulating an isolated cleavage plane.

Figure 4 shows the calculated total electron density in a (010) plane for $S=7.36$ a.u. and the figure shows no major differences from the theoretical results for this surface as reported by Wimmer, Neckel, and Freeman.[10] It is worth noting the large charge corrugation near the surface, and the rapidity with which even this four-layer slab acquires a bulklike electron density away from the surface. This suggests that four layers is not an unreasonable choice for the width of the slabs. While the four-layer width appears to be quite adequate for obtaining net charge densities and the energetics of separation (a comparison was made to separation into single-layer slabs), the detailed behavior of individual surface states, such as those given below, may be distorted by the thin width of the layers. The calculated work function is 4.6 eV, which compares well with the calculated value of Ref. 10, of 4.7 eV. Experimental values[11] are much lower, however, being about 3.8–4.1 eV. The most likely explanation for the difference is that the experimental results are lower due to the presence of carbon vacancies at the surface.[12] Figure 5 shows our muffin-tin sphere, angular-momentum projected, density of states (DOS), separated

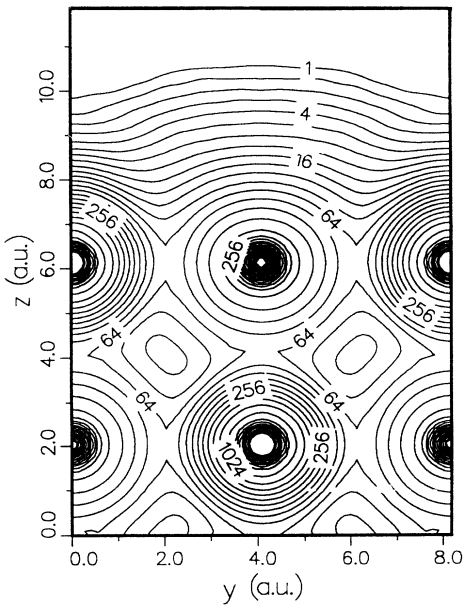

FIG. 4. The total electron density in a (010) plane at a (001) surface of the four-layer slab of Fig. 3 with $S=7.36$ a.u. The units are in 1×10^{-3} e/a.u.^{3}. The center atom at the surface is carbon.

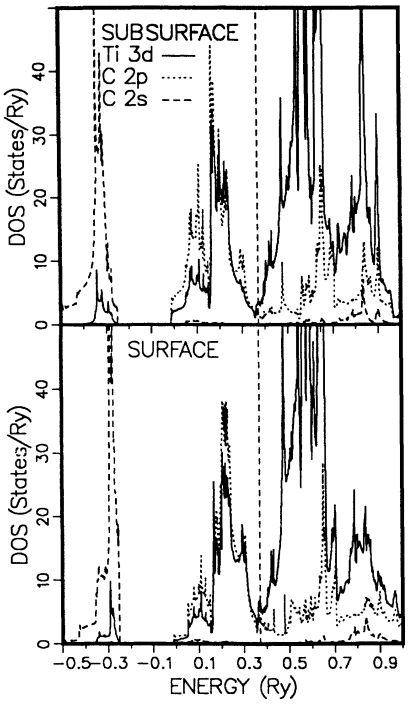

FIG. 5. The density of states in the four-layer slab, weighted by angular-momentum projected charge in the muffin-tin spheres. The dashed vertical line is at the Fermi energy.

into surface and subsurface layers. (These may be compared to the calculated bulk density of states shown in Figs. 2 and 3 of Ref. 6.) The surface electronic structure indicated by this graph has relevance both to the cleavage process and to the factors which select the (001) surface as the cleavage plane.

The most obvious reason for (001) cleavage planes in TiC is that these planes simply have the lowest number of broken carbon-metal nearest neighbor bonds per unit area. It is these bonds which dominate the cohesive behavior of the bulk carbides; however, the detailed nature of bond disruption at cleaved surfaces must also be considered. Figure 5 shows that all of the occupied valence states in TiC, including those with appreciable charge at the surface, exhibit a large amount of carbon-metal covalent bonding, with a Fermi level falling at a minimum in the DOS separating bonded and antibonded states. Thus, while the density of states of the occupied valence states shows some modifications due to the surface, broken bonds at the surface appear to be largely replaced by other bonding states (essentially by surface states which have bonding orbitals oriented parallel to the surface[7]) which reduces the energy required to create the surface. While this may also be true for other surfaces [e.g., (110) and (111)], at the (001) surface each surface atom loses only one of six nearest neighbors, which no doubt results in the least increase in the eigenvalues of the low-energy bonding orbitals. The cleavage process can then be qualitatively described as one which replaces covalent bonds across the opening interface with bonds directed along the surface.

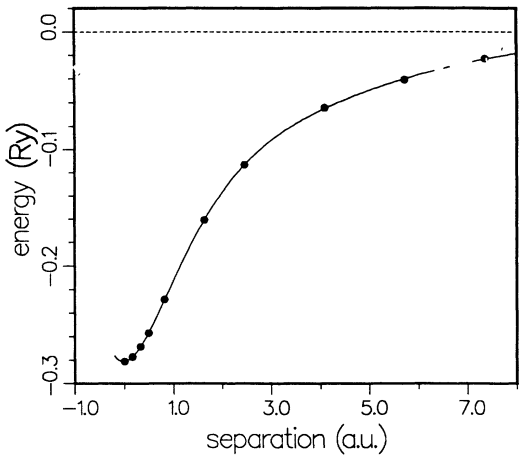

FIG. 6. Energy vs separation (S) for the atomic arrangement shown in Fig. 3. The solid line is again a least-squares fit and the dashed line is the asymptotic value of the fitted curve.

Figure 6 shows the calculated total energy of the four-layer unit cell as a function of excess separation (S in Fig. 3) between neighboring slabs. The curve is qualitatively just what one would expect, and fitting a simple function (cubic polynomial times an exponential) by nonlinear least squares gives values for the central quantities of a fracture calculation. The cleavage energy is found to be 8.4×10^{-3}Ry/a.u.^{2} (6545 erg/cm^2) and the surface energy is then half of this. The inflection point is the point of maximum stress in this separation process and occurs at a separation of 0.88 a.u., with a value for the maximum stress of 4.0×10^{11} dyn/cm^2. Either the value of the separation at the point of maximum stress or use of the calculated bulk stress-strain relationship (from Sec. II A) implies that the corresponding maximum strain is a very large 22%. This large value for the maximum strain points out the weakness in this calculation of the ideal yield stress in that this fracture process is calculated using the equilibrium values of the c and a lattice constants, while the prediction is that the fracture of the ideal crystal occurs at a c lattice constant 22% larger than this. Section II C below describes our calculation of the ideal stress and strain taking the stretching before fracture into account. Nonetheless, the calculation of the separation forced at the equilibrium lattice constants provides the simplest way of viewing the cleavage process, and so we shall now examine it in some more detail.

While the form of the energy versus separation curve of Fig. 6 contains nothing surprising,[13] what is of interest is how the length and energy scales of this curve are related to the breaking and rearrangement of electronic bonds at the interface. In order to obtain some feeling for this we present below a detailed view of certain states in the repeated slab system as the slabs are pulled apart. We have chosen for this purpose to confine our examination to states at the X point, at the center of the edge of the two-dimensional square Brillouin zone, since these most completely exhibit the carbon-metal covalent bonds which characterize the transition-metal carbides. Of these states we shall concentrate only on the four occu-

pied states with the highest energy. (The total symmetry group of the four-layer slabs contains asymmorphic symmetry operations; and this, combined with the fact that X lies on the boundary of the zone, results in all states at the X point being doubly degenerate. Consequently, there are only six independent eigenvalues in the carbon-p–titanium-d bonding band of states. The lowest two of these six states are dominated as much by carbon-p–carbon-p bonds as by carbon-metal bonds, and these bonds at the X point are directed parallel to the surface. As a result, while these states are among the lowest-energy bonding states in TiC which, from Fig. 5, appear to be most disrupted by the surface, the nature of these two states is quite nearly undisturbed by the separation; and consequently we do not show the behavior of these two states. Also, the carbon $2s$ band is a narrow, almost corelike band, and has little to do with the cohesive properties of TiC; so we do not show these states either.) Figure 7(a) shows the one-electron eigenvalues of these four states (relative to the Fermi energy) as a function of separation and it can be seen that all four of these states rise in energy relative to the Fermi energy, but that one of them (designated by open circles in the diagram) first drops and then rises much more sharply than the others. Figure 7(b) shows the relative distribution of the charge in these four states by plotting the net electron density of each state in the surface muffin-tin spheres minus the density in the center (subsurface) spheres as a function of separation. One of the states (solid squares) becomes strongly localized in the surface layers while another state (open squares) is strongly excluded from the surface regions. The remaining two states also separate into a surface-dominated and surface-excluded pair, although not as markedly so.

The next set of four figures (Figs. 8–11) give the charge density of each of these four states in a (010) plane for several values of the separation. (The double degeneracy

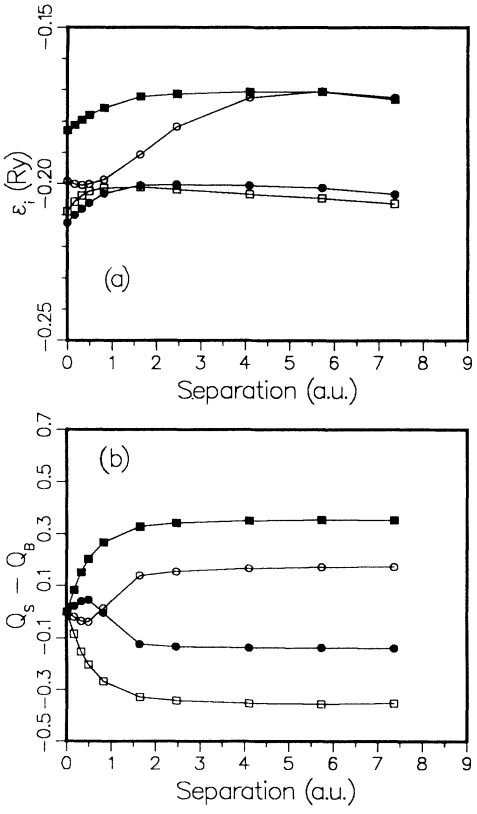

FIG. 7. (a) Eigenvalues of the four occupied states at X nearest the Fermi energy as a function of slab separation and (b) their net electron density in the surface layer muffin-tin spheres minus the net density in the subsurface muffin-tin spheres as a function of separation.

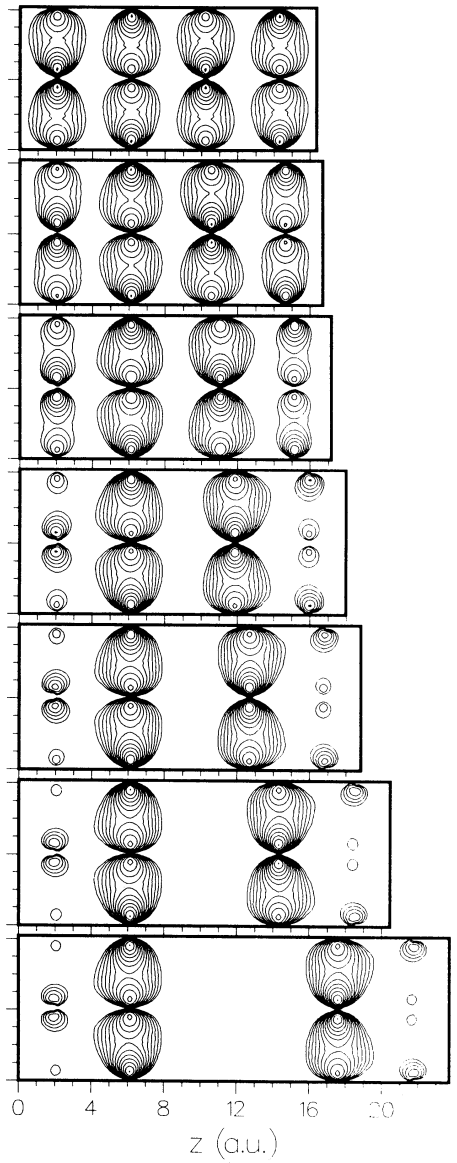

FIG. 8. The electron density in a (010) plane for the state labeled by solid squares in Figs. 7(a) and 7(b). In these figures, neighboring contours differ in density by a factor of square root of 2; and the location of the atoms is such that the leftmost atom along the center line is a titanium, next along the center line is carbon, etc. In this and Figs. 9–11 the slab separations are, from top to bottom, 0.00, 0.33, 0.82, 1.64, 2.45, 4.09, and 7.36 a.u..

of each of these states gives a great deal of freedom in arranging their appearance. The linear combination of the degenerate states has been chosen to give the maximum symmetry to the charge density in these figures.) We begin with the states labeled by squares in Figs. 7(a) and 7(b), which separate most strongly into surface and "antisurface" states (shown in Figs. 8 and 9, respectively). In the bulk configuration (no separation), both of these states are dominated by titanium-carbon bonds which run parallel to the (001) surface and so separation of the slabs breaks no covalent bonds. As a result, they separate into their final configuration very quickly (they appear to have nearly their final form long before the separation reaches that corresponding to maximum stress) and with relatively little increase in their eigenvalues.

The electron density of the state labeled by solid circles in Figs. 7(a) and 7(b) is shown in Fig. 10. It is clear from the figure that this state, in the bulk configuration, is the quintessential example of carbon-metal covalent bonding in the carbides and that separation of the slabs will break bonds across the interface. Figure 10 shows that, as the separation progresses, this state "hangs on" across the interface much longer than the previous two states examined, with the bonding charge stretching across the interface even at separations corresponding to the point of maximum stress, and "breaking" at some point after that. The appearance of the state changes rapidly somewhere between separations of 0.82 and 1.64 a.u., as it becomes largely excluded from the surface regions. The increase in the eigenvalue of this state, however, is not significantly greater than that of the previous two states. The state which did show a large increase in eigenvalue (after first decreasing) is the state labeled by open circles, which is shown as a function of separation in Fig. 11.

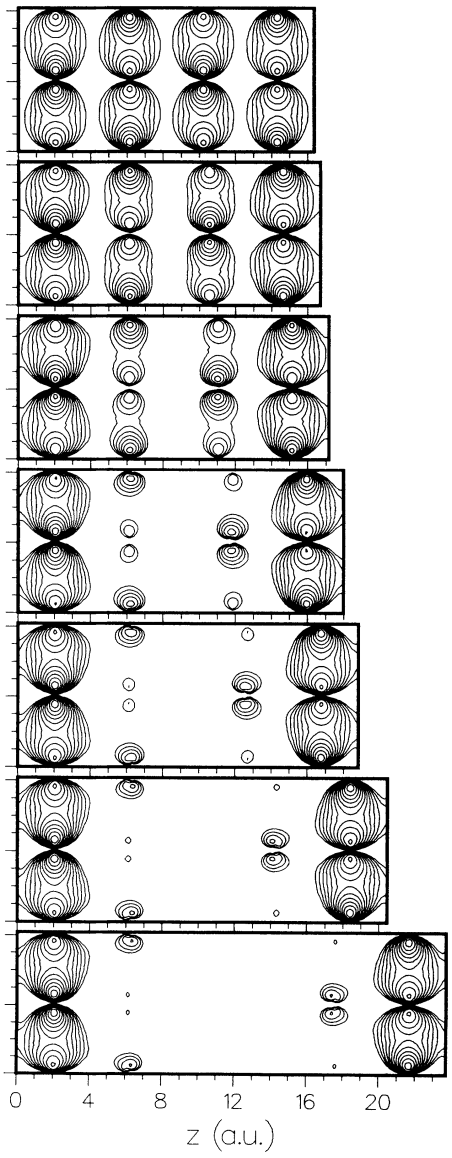

FIG. 9. Same as Fig. 8, for the state labeled by open squares in Figs. 7(a) and 7(b).

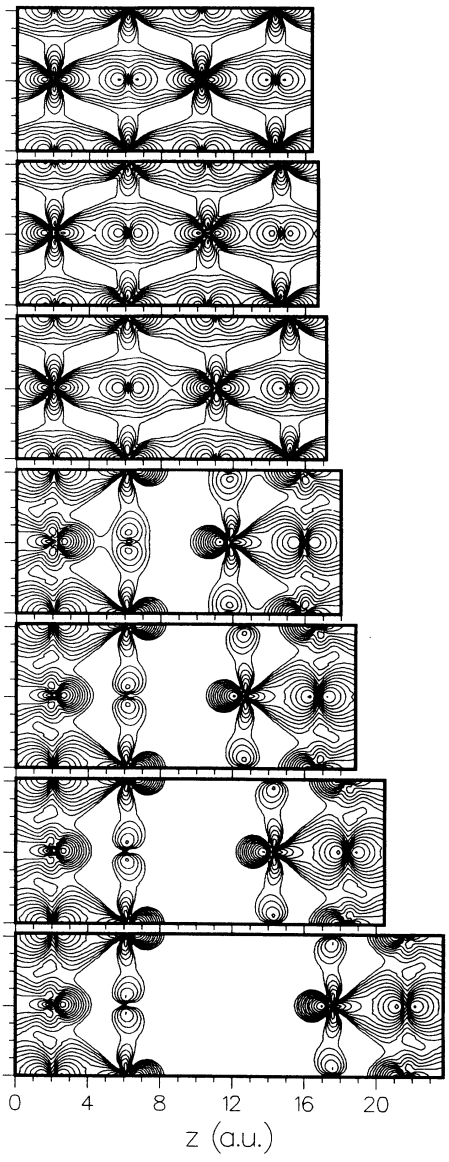

FIG. 10. Same as Fig. 8, for the state labeled by solid circles in Figs. 7(a) and 7(b).

While its bonding character may be difficult to distinguish in the bulk configuration in these figures, it is essentially a pi bonded state between carbon and titanium atoms lying in adjacent (001) planes. Indeed, these states have nodes in the density along each (001) plane of atoms with all of the bonding charge between (001) planes. It is clear from the figures why the eigenvalue first decreases: the bonding orbitals become visibly less cramped at a separation of about 0.3 a.u. corresponding roughly to the point of minimum eigenvalue. As the separation continues to increase the state becomes concentrated in the surface layers, and this occurs at about the same separation at which the third state (Fig. 10) left the surface regions. At this point the trans-surface bonding charge is definitely still intact and this remains true out to remarkably large separations, well beyond the point of maximum stress. At very large separations (somewhere between 2.45 and 4.09 a.u.) the lowest density contour is finally completely separated, and the state has become a surface state characterized by carbon-titanium pi bonding along the surface layer. From Fig. 7(a), the eigenvalue of this state rises close to its final value at a separation of about 3–4 a.u. We suggested above that the creation of surface states, such as the one shown in Fig. 11, limited the cleavage energy to a lower value than one might otherwise expect. Our overall discussion of Figs. 8–11 tends to confirm that it is such transformations of bulk states into surface states that dominates the energy versus separation variation.

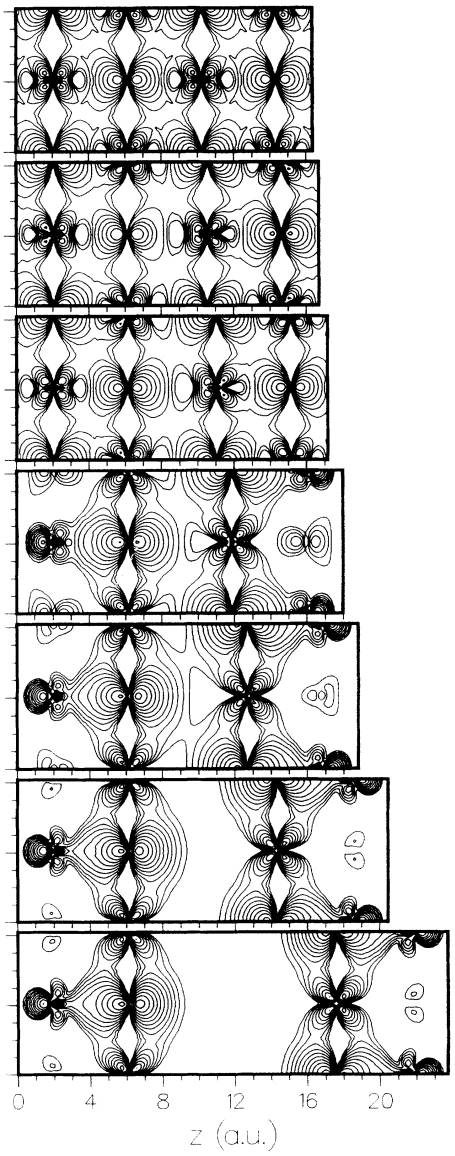

FIG. 11. Same as Fig. 8, for the state labeled by open circles in Figs. 7(a) and 7(b).

C. Ideal yield stress

It was noted in Sec. II B that the maximum stress obtained in that section was not, in principle, a proper determination of the ideal stress, since it was a calculation of the maximum stress required to separate two planes, with the other planes and the a lattice constant remaining at the unstrained values. In fact, what happens, in practice (or what would happen if there were no imperfections in the crystal), is that, as tensile stress is applied, the crystal at first simply stretches to a new c lattice constant (and a smaller a lattice constant). Any finite amount of strain causes an infinite sample to then be only metastable, although it is apparent that the effective barrier to a fractured state is quite formidable. For a perfect crystal, this stress (or strain) can continue to increase until the situation of metastable equilibrium (at equal planar spacing) against fracture turns into a point of unstable equilibrium. If it is assumed that the mode of failure of an ideal crystal under tensile ([001]) stress is simply the separation of adjacent (001) planes, then the point of fracture is reached when the second partial derivative of the total energy with respect to a single planar separation, evaluated with the remainder of the crystal at the "stretched" values of c and a, goes through zero and becomes negative. Thus, a calculation of the ideal yield stress, in principle, involves calculating the second derivative of the total energy with respect to a single plane separation as a function of c and a values corresponding to the stretched system. With the repeated slab construction, the idea is then to choose a range of values for c, determine the corresponding value of a (using the results of Sec. II A above), and then calculate the second derivative of the total energy with respect to slab separation, again with not a single isolated separation, but one repeated every four layers. Identification of the value of c at which the second derivative goes through zero, coupled with the results of Sec. II A, gives the ideal stress and strain. The same uncertainties apply here regarding the evaluation of second derivatives of the total energy as discussed in Sec. II A, so that this determination of the ideal yield stress may not in the end be any improvement over the value obtained in Sec. II B, but it is rewarding to at least attempt a proper calculation of the ideal yield stress. Figure 12 shows the calculated second derivative of the total energy with respect to slab separation as a function of the c lattice constant (where the corresponding a lattice constant was determined using the results

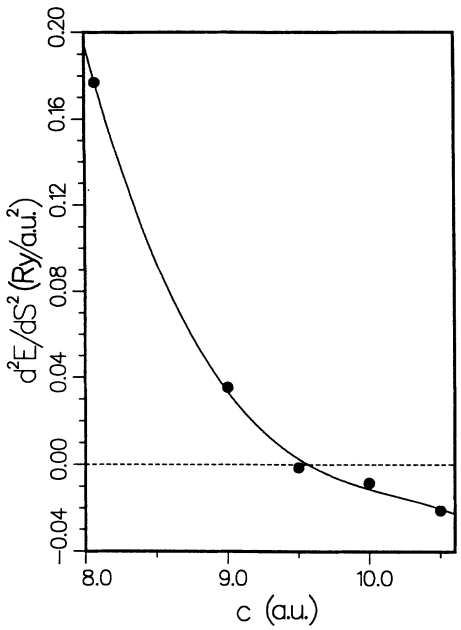

FIG. 12. Second derivative of total energy with respect to separation as a function of the c lattice constant. The solid line is a least-squares-fitted cubic polynomial.

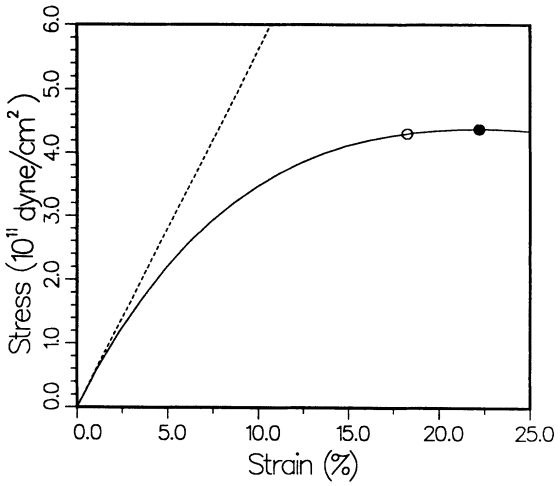

FIG. 13. The calculated stress vs strain for [001] stress in TiC. The dashed line corresponds to the value of Young's modulus found in Sec. II A, the solid circle is the point of maximum stress (where infinite stretching occurs), and the open circle marks the calculated stress and strain at which brittle fracture occurs.

shown in Fig. 1). A cubic polynomial fitted to these points gives the point of fracture at a strain of 18% ($c=9.6$ a.u.), and using the results of Fig. 2, this gives an ideal yield stress of 4.3×10^{11} dyn/cm^2.

The summary result of these calculations of TiC under tensile stress is presented in Fig. 13. This is a graph of the calculated stress versus strain relationship, obtained by taking the derivative of the energy-strain curve presented in Fig. 2. The point of maximum stress labeled by the solid circle is the point where we find the stretched crystal is unstable with respect to unlimited stretching, and the point labeled by the open circle is the calculated strain at which ideal TiC will fracture along its (001) planes.

III. SUMMARY

The calculations described above have examined the cleavage of ideal TiC along (001) planes in a detailed manner and have arrived at a theoretical description of the behavior of TiC under tensile stress, examining both the elastic and inelastic behavior. While the determination of the elastic constants was within reasonable agreement with experimental results, the determination of the stress at which fracture occurs, as expected, gives a value which is several times larger than obtained even under carefully controlled conditions. Rough estimates of ideal yield stress are often in terms of Young's modulus, with the ratio of yield stress to Young's modulus being estimated[3] at about 10 or 20. Our calculations support these estimates, in that we obtain a ratio of yield stress to Young's modulus of about 13. The results presented in Figs. 8–11 and the accompanying discussion in Sec. II B, provide a detailed pictorial analysis of the charge redistribution accompanying cleavage.

ACKNOWLEDGMENTS

The research at West Virginia University was supported by Air Force Office of Scientific Research Grant No. AFOSR-87-0251, and the research at Los Alamos National Laboratory was supported by the U.S. Department of Energy.

[1]L. E. Toth, *Transition Metal Carbides and Nitrides* (Academic, New York, 1971).
[2]J. Gilman and B. Roberts, J. Appl. Phys. **32**, 1405 (1961).
[3]J. F. Knott, *Fundamentals of Fracture Mechanics* (Butterworths, London, 1973).
[4]D. D. Vvedensky, S. Crampin, M. E. Eberhart, and J. M. MacLaren, Contemp. Phys. **31**, 73 (1990).
[5]O. K. Anderson, Phys. Rev. B **12**, 3060 (1975).
[6]D. L. Price and B. R. Cooper, Phys. Rev. B **39**, 4945 (1989).
[7]D. L. Price, J. M. Wills, and B. R. Cooper (unpublished).
[8]A. Dunand, H. D. Flack, and K. Yvon, Phys. Rev. B **31**, 2299 (1985).
[9]R. Chang and L. J. Graham, J. Appl. Phys. **37**, 3778 (1966).
[10]E. Wimmer, A. Neckel, and A. J. Freeman, Phys. Rev. B **31**, 2370 (1985).
[11]C. Oshima, T. Tanaka, M. Aono, R. Nishitani, S. Kawai, and F. Yajima, Appl. Phys. Lett. **35**, 822 (1979); P. Lindberg and L. Johansson, Surf. Sci. **194**, 199 (1988).
[12]G. R. Gruzalski, S.-C. Liu, and D. M. Zehner, Surf. Sci. **239**, L517 (1990); D. L. Price and B. R. Cooper, Bull. Am. Phys. Soc. **35**, 602 (1990); D. L. Price, B. R. Cooper, and J. M. Wills (unpublished).
[13]A. Banerjea and J. Smith, Phys. Rev. B **37**, 6632 (1988).